

- chemistry* **35**, 4966 (1996).
10. J.-K. Hériché, F. Lebrin, Y. Goldberg, unpublished data.
 11. S. Colley, H. Paterson, P. Kemp, C. J. Marshall, *Cell* **77**, 841 (1994); S. J. Mansour *et al.*, *Science* **265**, 966 (1994); G. Pagès, A. Brunet, G. L'Allemain, J. Pouyssegur, *EMBO J.* **13**, 3003 (1994).
 12. R. Pepperkok, P. Lorenz, R. Jakobi, W. Ansoorge, W. Pyerin, *Exp. Cell Res.* **197**, 245 (1991); I. Roussou and G. Draetta, *Mol. Cell. Biol.* **14**, 576 (1994); V. Snell and P. Nurse, *EMBO J.* **13**, 2066 (1994); D. E. Hanna, A. Rethinaswamy, C. V. C. Glover, *J. Biol. Chem.* **270**, 25905 (1995).
 13. D. C. Seldin and P. Leder, *Science* **267**, 894 (1995); M. A. Kelliher, D. C. Seldin, P. Leder, *EMBO J.* **15**, 5160 (1996).
 14. NIH 3T3 cells (1.5×10^6) were transfected with Lipofectamine (Gibco) with 18 μ g of the relevant CK2 α -HA expression vector (6), serum-deprived for 20 hours, then lysed in 1 ml of buffer B [20 mM tris-HCl (pH 7.4), 50 mM NaCl, 50 mM NaF, 1% Triton X-100, 14 mM β -mercaptoethanol, aprotinin (25 μ g/ml), leupeptin (25 μ g/ml), 100 nM okadaic acid, and 0.1 mM activated vanadate]. Clarified lysates were immunoprecipitated with 1 μ l of monoclonal antibody (12CA5) to HA and 25 μ l of protein A-Sepharose. Immunoprecipitates were washed three times in buffer B and once in tris-buffered saline [20 mM tris-HCl (pH 7.4), 150 mM NaCl] containing 100 nM okadaic acid and subjected to chemiluminescent immunoblotting.
 15. PP2A (500 ng) was incubated at 30°C for 20 min with 5 ng of GST-CK2 α in 30 μ l of kinase buffer containing 100 μ M [γ -³²P]ATP (10^4 dpm/pmol) and okadaic acid (1 μ M). Then, 30 μ l of 2% SDS was added, the mixture was heated at 100°C for 5 min, diluted into 540 μ l of 20 mM tris-HCl (pH 7.4), 150 mM NaCl, 1% Triton X-100, 0.5% sodium deoxycholate, and BSA (1 mg/ml), and immunoprecipitated with 2 μ l of anti-PP2Ac.
 16. Immunoprecipitates (14) were prepared without okadaic acid and incubated with 60 ng of the Raf1-phosphorylated MEK1 at 20°C in 30 μ l of kinase buffer without MgCl₂. Reactions were analyzed by SDS-polyacrylamide gel electrophoresis (PAGE) and autoradiography.
 17. C. S. Gibbs and M. J. Zoller, *J. Biol. Chem.* **266**, 8923 (1991); I. Mikaelian and A. Sergeant, *Nucleic Acids Res.* **20**, 376 (1992).
 18. Wild-type and mutant chicken CK2 α cDNAs were subcloned (as HA-tagged derivatives) in frame with GST and expressed in *Escherichia coli* BL21(DE3). GST fusions were purified by glutathione-Sepharose chromatography as recommended by the manufacturer (Pharmacia). The purified GST fusions (200 ng) were incubated with purified PP2A dimer (200 ng, UBI) in 100 μ l of kinase buffer for 20 min at 25°C. The mixture was adsorbed to glutathione-Sepharose in buffer A [20 mM tris-HCl (pH 7.4), 50 mM NaCl, 0.1% Triton X-100, 14 mM β -mercaptoethanol] for 30 min at 4°C. The beads were washed three times in buffer A, eluted into Laemmli buffer, and analyzed by chemiluminescent immunoblotting.
 19. E. T. Ulug, A. J. Cartwright, S. A. Courtneidge, *J. Virol.* **66**, 1458 (1992).
 20. CK2 β was subcloned into the pMAL vector (New England Biolabs), expressed as a maltose-binding protein (MBP)-CK2 β fusion, and purified by chromatography on amylose beads.
 21. PP2A dimer (10 ng, 20 mU) was incubated for 15 min at 30°C with GST-CK2 α (2 ng), with or without 100 μ M ATP. Bacterially produced His-MEK1 (100 ng) that had been ³²P-labeled in vitro by immunoprecipitated Raf [J. R. Fabian, A. B. Vojtek, J. A. Cooper, D. K. Morrison, *Proc. Natl. Acad. Sci. U.S.A.* **91**, 5982 (1994)] and repurified was added and incubated for a further 15 min. Reactions were directly analyzed by SDS-PAGE and PhosphorImager quantitation of the His-MEK1 bands.
 22. All probabilities were computed by Student's *t* test with Scheffe's correction for multiple comparisons.
 23. Immunoprecipitates were incubated for 15 min at 25°C in 30 μ l of kinase buffer containing 20 μ M [γ -³²P]ATP (10^4 dpm/pmol). Reactions were stopped by adding Laemmli gel buffer and heating at 100°C. For reimmunoprecipitation (15), 10 μ M [γ -³²P]ATP (10^5 dpm/pmol) was used.
 24. Cells were transfected with Lipofectamine with 6 μ g of plasmid per 0.5×10^6 cells. All lysates were immunoprecipitated with 1 μ l of 12CA5 and assayed for 10 min as above (16).
 25. T. Rabilloud, C. Valette, J. J. Lawrence, *Electrophoresis* **15**, 1552 (1994).
 26. O. Filhol, C. Cochet, E. M. Chambaz, *Biochemistry* **29**, 9928 (1990).
 27. Cells (1.5×10^6) were transfected by calcium phosphate precipitation with a mixture of 2 μ g of CK2 α , 8 μ g of His-MEK1, and 12 μ g of carrier plasmid. Cells were lysed in buffer B containing 100 mM NaCl (14), and His-MEK1 was adsorbed onto 20 μ l of nickel-trinitrioloacetate resin (Invitrogen) for 1 hour at 4°C, washed three times in lysis buffer, and eluted into 50 μ l of lysis buffer containing BSA (1 mg/ml) and 0.25 M imidazole (pH 7.4).
 28. We thank S. A. Courtneidge for anti-PP2A and peptide; A. Brunet and J. Pouyssegur for the HA-MAPK and MEK2 constructs; U. R. Rapp for anti-Raf; J. Ghysdael for the Raf1 baculovirus; T. Sturgill for the SrcF527 and v-Ha-Ras baculoviruses; A. Berns and C. Ovitv for the pGKHgryo plasmid; and J. Ghysdael, D. Job, and our laboratory colleagues for critically reviewing the manuscript. J.-K.H. was supported by the Ministère de l'Enseignement Supérieur et de la Recherche and by the Ligue Nationale contre le Cancer. Supported by Commissariat à l'Energie Atomique, INSERM, and CNRS.

25 June 1996; accepted 5 March 1997

Structures of the Tyrosine Kinase Domain of Fibroblast Growth Factor Receptor in Complex with Inhibitors

Moosa Mohammadi, Gerald McMahon, Li Sun, Cho Tang, Peter Hirth, Brian K. Yeh, Stevan R. Hubbard,* Joseph Schlessinger*

A new class of protein tyrosine kinase inhibitors was identified that is based on an oxindole core (indolinones). Two compounds from this class inhibited the kinase activity of fibroblast growth factor receptor 1 (FGFR1) and showed differential specificity toward other receptor tyrosine kinases. Crystal structures of the tyrosine kinase domain of FGFR1 in complex with the two compounds were determined. The oxindole occupies the site in which the adenine of adenosine triphosphate binds, whereas the moieties that extend from the oxindole contact residues in the hinge region between the two kinase lobes. The more specific inhibitor of FGFR1 induces a conformational change in the nucleotide-binding loop. This structural information will facilitate the design of new inhibitors for use in the treatment of cancer and other diseases in which cell signaling by tyrosine kinases plays a crucial role in disease pathogenesis.

Protein tyrosine kinases (PTKs) are critical components of signaling pathways that control cell proliferation and differentiation. Enhanced PTK activity due to activating mutations or overexpression has been implicated in many human cancers (1). Thus, selective inhibitors of PTKs have considerable therapeutic value (2). Although a number of compounds have been identified as effective inhibitors of specific PTKs, the precise molecular mechanisms by which these agents inhibit PTK activity have not been elucidated.

Fibroblast growth factors (FGFs) play important roles in embryonic development, angiogenesis, wound healing, and malignant transformation (3). The diverse effects of mammalian FGFs are mediated by four

transmembrane receptors (FGFR1 through FGFR4) with intrinsic PTK activity (4). Activating mutations in FGF receptor genes have been implicated in various human skeletal disorders such as Crouzon syndrome (5), achondroplasia (6, 7), and thanatophoric dysplasia (7, 8). Inappropriate expression of FGFs or activation of FGF receptors could contribute to several human angiogenic pathologies such as diabetic retinopathy, rheumatoid arthritis, atherosclerosis, and tumor neovascularization (9). Moreover, genes encoding FGFR1 and FGFR2 were shown to be amplified in a population of breast cancers (10). Overexpression of FGF receptors has also been detected in human pancreatic cancers (11), astrocytomas (12), salivary gland adenocarcinomas (13), Kaposi's sarcomas (14), ovarian cancers (15), and prostate cancers (16).

We identified a new family of inhibitors for receptor tyrosine kinases by screening a library of synthetic compounds. A new class of PTK inhibitors was generated by attaching different chemical substituents to an oxindole core (indolinones). These com-

M. Mohammadi, B. K. Yeh, J. Schlessinger, Department of Pharmacology, New York University Medical Center, New York, NY 10016, USA.
G. McMahon, L. Sun, C. Tang, P. Hirth, SUGEN, Redwood City, CA 94063, USA.
S. R. Hubbard, Skirball Institute of Biomolecular Medicine and Department of Pharmacology, New York University Medical Center, New York, NY 10016, USA.

*To whom correspondence should be addressed.

pounds were then tested for their ability to inhibit the PTK activity of FGFR1 in NIH 3T3 cells. The chemical structures of two compounds that were used in subsequent studies, 3-[4-(1-formylpiperazin-4-yl)-benzylidene]-2-indolinone (SU4984) and 3-[(3-(2-carboxyethyl)-4-methylpyrrol-2-yl)methylene]-2-indolinone (SU5402), are shown in Fig. 1A (17).

We examined the effect of these inhibitors on the activity of the purified kinase domain of FGFR1 (FGFR1K). An *in vitro* autophosphorylation assay was done with FGFR1K in the presence of various concentrations of SU4984 or SU5402 (18). Both compounds inhibited the kinase activity of FGFR1K with a median inhibitory concentration (IC_{50}) of 10 to 20 μ M in the presence of 1 mM adenosine triphosphate (ATP) (Fig. 1B). This experiment demonstrated that the inhibitory effects of the two compounds are due to direct interactions of these inhibitors with the catalytic domain of FGFR1.

Next, we compared the capacity of these two compounds to block the kinase activity of FGFR1 in living cells (Fig. 1C) (19). NIH 3T3 cells were treated with the compounds, then stimulated with acidic FGF (aFGF). The cells were lysed, and proteins were immunoprecipitated with antibodies to FGFR1, separated by SDS-polyacryla-

mid gel electrophoresis (PAGE), immunoblotted with antibodies to phosphotyrosine, and detected by autoradiography. Autophosphorylation of FGFR1 induced by aFGF was inhibited by the two compounds with IC_{50} 's of 20 to 40 μ M for SU4984 and 10 to 20 μ M for SU5402. These two compounds also inhibited (with similar IC_{50} 's) aFGF-induced tyrosine phosphorylation of a 90-kD phosphoprotein (pp90) and mitogen-activated protein (MAP) kinases (ERK1 and ERK2), two intracellular events that are dependent on the kinase activity of FGFR1 (Fig. 1D). Both compounds also inhibited [3 H]thymidine incorporation in response to aFGF stimulation (Fig. 1E) (20).

In similar experiments, SU4984 inhibited tyrosine phosphorylation of the platelet-derived growth factor (PDGF) receptor and of the insulin receptor (Fig. 2A) (21). In contrast, SU5402 did not inhibit tyrosine phosphorylation of the insulin receptor and was only a weak inhibitor of phosphorylation of the PDGF receptor (Fig. 2A). Neither compound inhibited the kinase activity of the epidermal growth factor (EGF) receptor, even at an inhibitor concentration of 200 μ M. To examine the effects of the inhibitors on receptor-mediated signaling events, we subjected portions of the lysates from inhibitor-treated or untreated cells to SDS-

PAGE, followed by immunoblotting with antibodies to phosphotyrosine, and then autoradiography (Fig. 2B). Stimulation of NIH 3T3 cells with PDGF resulted in tyrosine phosphorylation of the PDGF receptor (p190) and phospholipase C γ (p150), and in activation of ERK2 (p42). Treatment of NIH3T3 cells with insulin resulted in strong tyrosine phosphorylation of the β subunit of the insulin receptor (p95) and IRS-1 (p185). Stimulation of HER14 cells with EGF led to tyrosine phosphorylation of the EGF receptor (p170) and the adaptor protein Shc (p52), and to activation of ERK2. Tyrosine phosphorylation of these downstream signaling proteins was inhibited by SU4984 and SU5402 in direct correlation with inhibition of receptor autophosphorylation (Fig. 2). Thus, the two inhibitors exhibit differential specificity toward these four receptor tyrosine kinases.

The three-dimensional structure of FGFR1K has been determined by x-ray crystallography (22). FGFR1K has a two-lobe architecture typical of protein kinases. ATP binds in the cleft between the two lobes (22, 23). For crystallographic studies of FGFR1K-inhibitor complexes, unliganded FGFR1K crystals were soaked in solutions containing either SU5402 or SU4984. Data collection and refinement

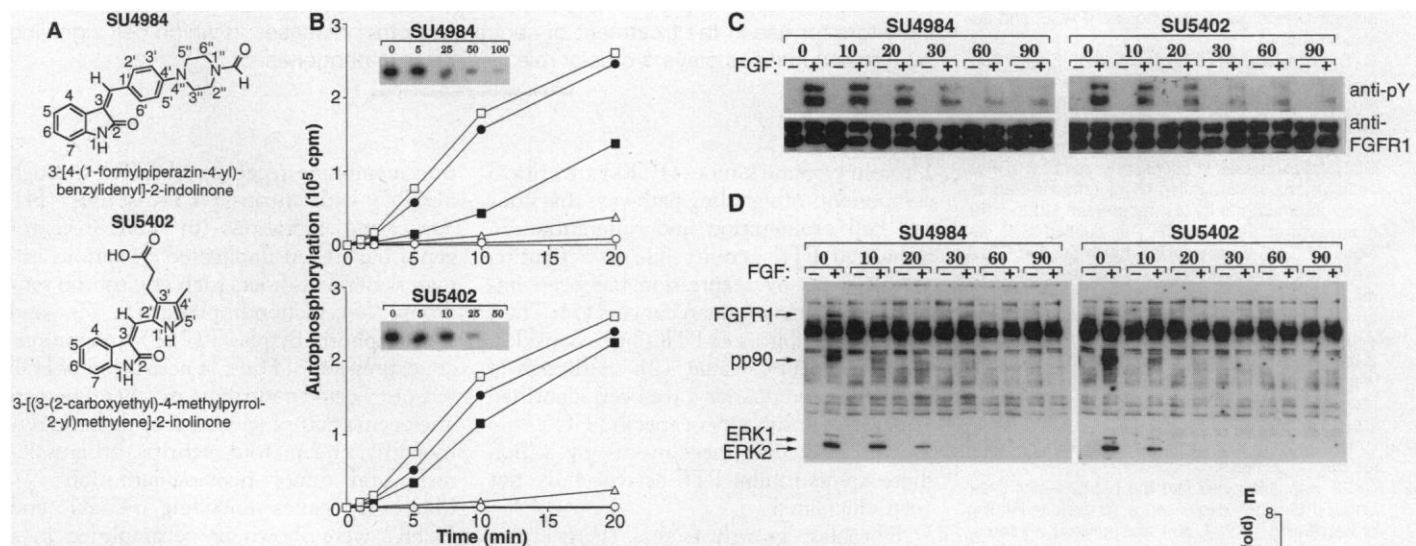


Fig. 1. Chemical structures and inhibitory properties of two oxindole-based compounds. **(A)** Chemical structures are shown for SU4984 and SU5402. **(B)** Inhibition of the PTK activity of FGFR1K *in vitro* by SU4984 and SU5402. The autophosphorylation activity of FGFR1K was determined in the presence of [γ - 32 P]ATP, MgCl $_2$, and various concentrations of the inhibitors. SU4984: 0 μ M \square , 5 μ M \bullet , 25 μ M \blacksquare , 50 μ M \triangle , 100 μ M \circ . SU5402: 0 μ M \square , 5 μ M \bullet , 10 μ M \blacksquare , 25 μ M \triangle , 50 μ M \circ . The autophosphorylation reaction was stopped at different times and the 32 P incorporation was quantitated. The autoradiograms of kinase reaction after 5 min are shown in the left corner of each graph. **(C)** Inhibition of FGFR1 autophosphorylation *in vivo*. NIH 3T3 cells were incubated with various concentrations (in micromolar) of the inhibitors for 5 min at 37°C and then stimulated with aFGF (100 ng/ml) and heparin (10 μ g/ml) (+) or left unstimulated (-) for 5 min at 37°C. Cell lysates were immunoprecipitated with antibodies to FGFR1, separated by SDS-PAGE, and immunoblotted with antibodies to phosphotyrosine (anti-pY) or FGFR1 (anti-FGFR1). **(D)** Inhibition of aFGF-induced tyrosine phosphorylation *in vivo*. Portions of the lysates from (C) were analyzed by SDS-PAGE and immunoblotted with antibodies to phosphotyrosine. The positions of FGFR1, pp90, ERK1, and ERK2 are indicated by arrows. **(E)** Inhibition of aFGF-induced [3 H]thymidine incorporation. Inhibitor-treated (50 μ M) or untreated (control) NIH 3T3 cells were stimulated with aFGF. The cells were then labeled with [3 H]thymidine and thymidine incorporation was measured after 24 hours.

statistics are given in Table 1. The electron density maps show good supporting density for all the atoms of SU5402 and for the atoms of the oxindole and the phenyl ring of SU4984, whereas the density is weaker for the atoms in the piperazine ring and the terminal formyl group of SU4984 (Fig. 3).

The inhibitors bind to FGFR1K in the same general region as ATP (Fig. 4). The oxindole of the inhibitors occupies the same site as the ATP adenine, although the orientations of the bicyclic ring systems differ by nearly 180° (Fig. 4, C and D). The chemical groups attached to C-3 of the oxindole emerge from the cleft at approximately right angles to the direction taken by the rest of the ATP molecule. Neither inhibitor binds near the putative substrate peptide binding site in the COOH-terminal lobe of the kinase, indicating that these inhibitors do not compete with substrate peptide.

The oxindole makes two hydrogen bonds to the protein backbone of FGFR1K: between N-1 of the oxindole and the carbonyl oxygen of Glu⁵⁶², and between O-2 of the oxindole and the amide nitrogen of Ala⁵⁶⁴ (Fig. 5). Glu⁵⁶² and Ala⁵⁶⁴ reside in the hinge region, the segment between β5 and αD (residues 563 through 568) that connects the two lobes of FGFR1K. These same two backbone groups of FGFR1K make hydrogen bonds to N-1 and N-6 of the ATP adenine (22). The cavity in which the oxindole (or adenine) binds is lined

with numerous hydrophobic residues including Val⁴⁹², Ala⁵¹², Ile⁵⁴⁵, Val⁵⁶¹, Ala⁵⁶⁴, and Leu⁶³⁰. In addition, Leu⁴⁸⁴ and Tyr⁵⁶³ provide a hydrophobic environment for the ring proximal to the oxindole—a phenyl in SU4984 and a pyrrole in SU5402 (Fig. 5).

The remainder of the interactions between the two inhibitors and FGFR1K differ. The phenyl ring of SU4984 makes an oxygen-aromatic contact (24) with the carbonyl oxygen of Ala⁵⁶⁴. The piperazine

ring of SU4984 is in van der Waals contact with Gly⁵⁶⁷, a highly conserved residue in protein kinases. The terminal formyl group of SU4984 has poor associated electron density, indicating that this group is disordered. Indeed, a compound lacking the formyl group is as potent an inhibitor as SU4984 (25). In the FGFR1K-SU5402 structure, N-1' of the pyrrole ring makes an intramolecular hydrogen bond with O-2 of the oxindole. The methyl group of the pyrrole ring is in

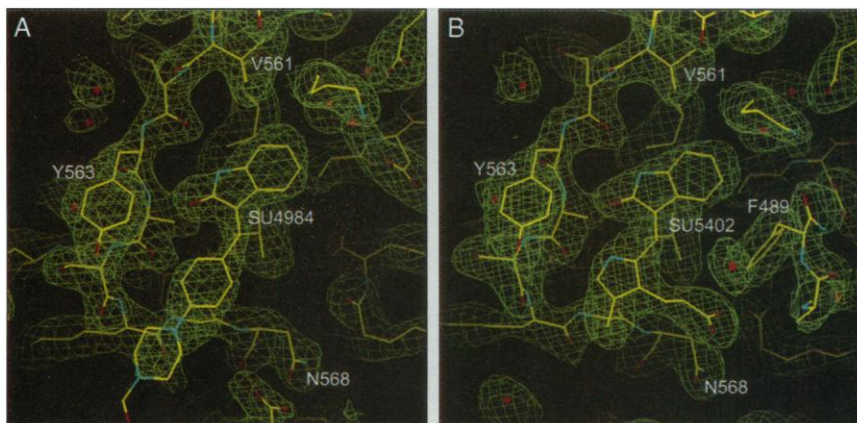


Fig. 3. $2F_o - F_c$ electron density maps computed after simulated annealing (1000 K) with the inhibitors omitted from the atomic models. Carbon atoms are colored yellow, oxygen atoms red, and nitrogen atoms blue. The red spheres represent water molecules. Maps are contoured at 1σ . (A) Map of FGFR1K-SU4984 computed at 2.4 Å resolution. (B) Map of FGFR1K-SU5402 computed at 2.5 Å resolution. Figure prepared with SETOR (34).

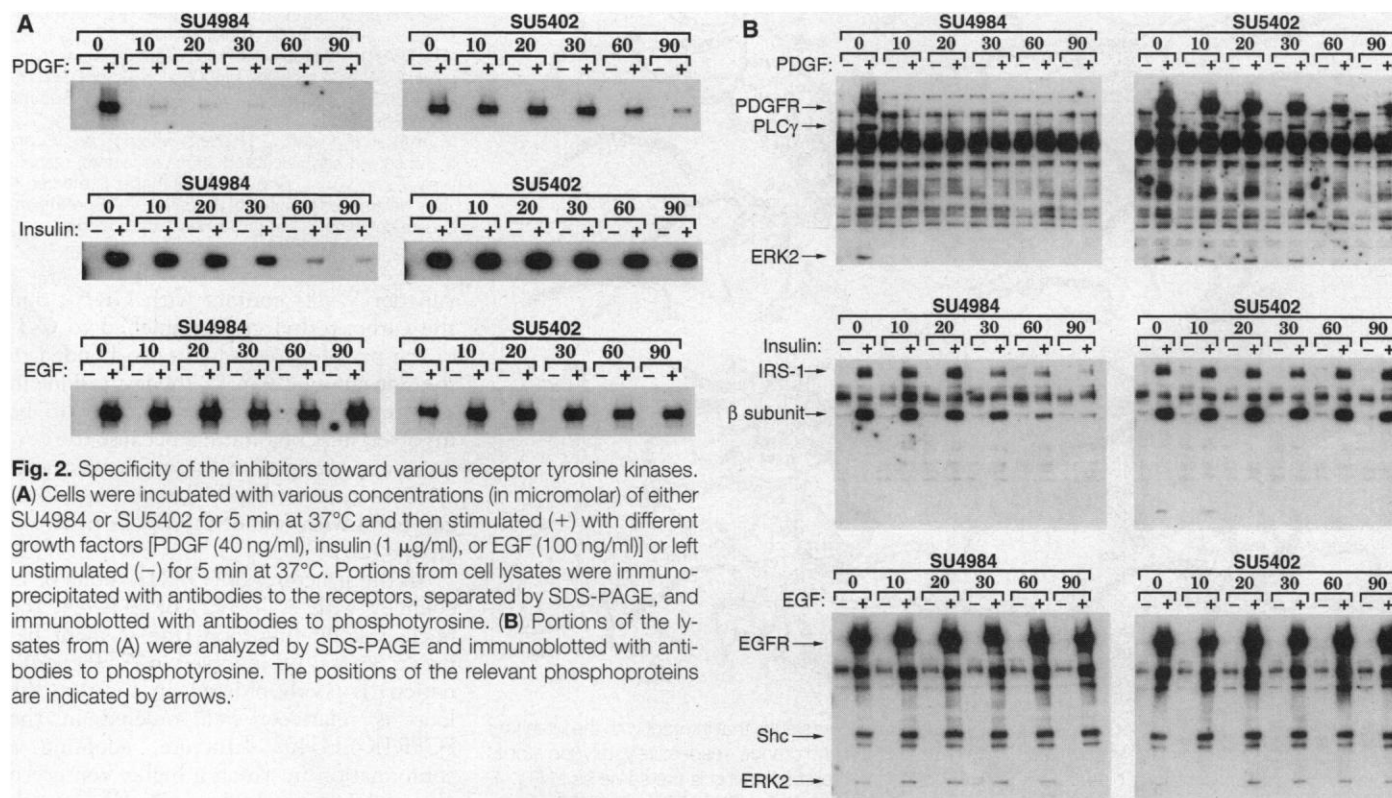


Fig. 2. Specificity of the inhibitors toward various receptor tyrosine kinases. (A) Cells were incubated with various concentrations (in micromolar) of either SU4984 or SU5402 for 5 min at 37°C and then stimulated (+) with different growth factors [PDGF (40 ng/ml), insulin (1 μg/ml), or EGF (100 ng/ml)] or left unstimulated (-) for 5 min at 37°C. Portions from cell lysates were immunoprecipitated with antibodies to the receptors, separated by SDS-PAGE, and immunoblotted with antibodies to phosphotyrosine. (B) Portions of the lysates from (A) were analyzed by SDS-PAGE and immunoblotted with antibodies to phosphotyrosine. The positions of the relevant phosphoproteins are indicated by arrows.

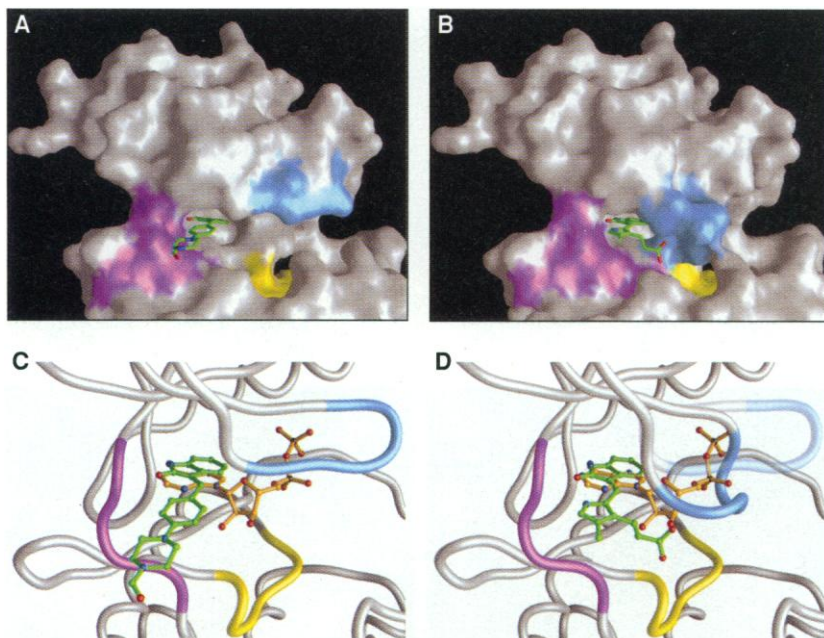


Fig. 4. Views of SU4984 and SU5402 bound to FGFR1K. **(A)** Molecular surface representation of FGFR1K shows SU4984 bound in the cleft between the two lobes of the kinase. The surface is colored purple for atoms of the FGFR1K hinge region, light blue for atoms of the nucleotide-binding loop, and yellow for atoms of the catalytic loop. **(B)** Representation is the same as (A) but for SU5402. **(C)** Superposition of SU4984 and ATP (22) bound to FGFR1K. Carbon atoms of SU4984 and ATP are green and orange, respectively; oxygen atoms are red, nitrogen atoms are blue, and phosphorus atoms are black. The γ phosphate of ATP is not shown because of disorder (22). Coloring of the backbone representation is the same as the surface coloring in (A). **(D)** Same as (C), but showing superposition of SU5402 and ATP bound to FGFR1K. To highlight the conformational change in the nucleotide-binding loop induced by SU5402, the loop as found in the FGFR1K-SU4984 structure is included (semitransparent). Figures 4, 5, and 6B prepared with GRASP (35).

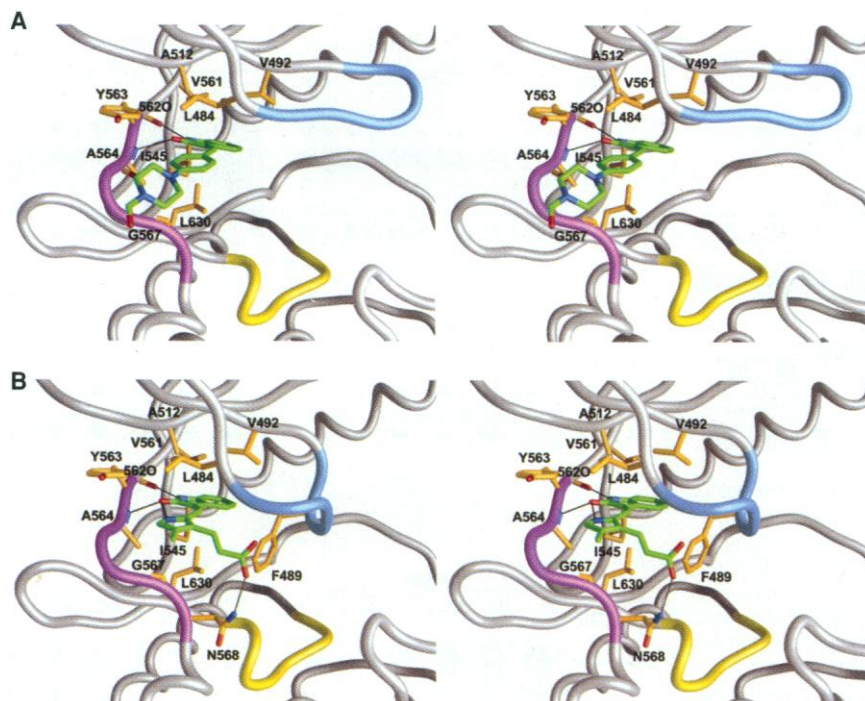


Fig. 5. Stereoviews of the inhibitor binding sites. The side chains of residues that interact with the inhibitors are shown. Carbon atoms of the inhibitor and FGFR1K are green and orange, respectively; oxygen atoms are red and nitrogen atoms are blue. Coloring of the backbone representation is the same as in Fig. 4. Selected hydrogen bonds are shown as black lines. **(A)** FGFR1K-SU4984. **(B)** FGFR1K-SU5402.

Table 1. Data collection and refinement. Expression, purification, and crystallization of FGFR1K were done as described (22). Crystals of native FGFR1K (space group C2, two molecules in the asymmetric unit) were soaked in 500 μ l of stabilizing solution [25% PEG 10000, 0.3 M $(\text{NH}_4)_2\text{SO}_4$, 0.1 M bis-tris (pH 6.5), and 5% ethylene glycol] containing SU4984 (5 mM) or SU5402 (1 mM) at 4°C for 24 to 48 hours. Data were collected on a Rigaku RU-200 rotating anode (Cu K α) operating at 50 kV and 100 mA and equipped with double-focusing mirrors and an R-Axis IIC image plate detector. One cryo-cooled crystal was used for each data set. Crystals were flash-cooled in a dry nitrogen stream at -175°C. Data were processed with DENZO and SCALEPACK (36). Difference Fourier electron density maps were computed using phases calculated from the structure of unliganded FGFR1K (22). X-PLOR (37) was used for simulated annealing (1000 K) and conjugate-gradient minimization, and TOM/FRODO (38) was used for model building. The average *B* factor for all atoms is 38.3 \AA^2 for FGFR1K-SU4984 and 39.2 \AA^2 for FGFR1K-SU5402.

Parameter	SU4984	SU5402
<i>Data collection statistics</i>		
Resolution (\AA)	20.0–2.4	20.0–2.5
Observations (<i>n</i>)	94093	93535
Completeness (%) [*]	99.1 (97.9)	97.6 (96.1)
Redundancy	3.3	3.7
<i>R</i> _{sym} (%) ^{*†}	6.3 (32.2)	6.8 (23.0)
Signal (<i>I</i> > σ <i>I</i>)	11.4	11.8
<i>Refinement statistics</i> [‡]		
Resolution (\AA)	6.0–2.4	6.0–2.5
Reflections (<i>n</i>)	23530	20402
<i>R</i> value (%) [§]	19.5 (28.1)	19.0 (27.0)
Bonds (\AA) [¶]	0.008	0.008
Angles ($^\circ$) [¶]	1.3	1.4
<i>B</i> factors (\AA^2) ^{¶#}	1.5	1.5

^{*}Value in parentheses is for the highest resolution shell. [†] $R_{\text{sym}} = 100 \times \sum_{hkl} \sum_i |I_i(hkl) - \langle I(hkl) \rangle| / \sum_{hkl} \sum_i I_i(hkl)$. [‡]For FGFR1K-SU4984: 550 residues, 234 water molecules, 2 SU4984 molecules (4608 atoms); for FGFR1K-SU5402: 550 residues, 229 water molecules, 2 SU5402 molecules (4636 atoms). [§] R value = $100 \times \sum_{hkl} | |F_o(hkl)| - |F_c(hkl)| | / \sum_{hkl} |F_o(hkl)|$, where F_o and F_c are the observed and calculated structure factors, respectively ($F_o > 2\sigma$). [¶]Value in parentheses is the free *R* value determined from 5% of the data. ^{¶¶}Root-mean-square deviation. [#]For bonded protein atoms.

van der Waals contact with Gly⁵⁶⁷, and the carboxyethyl group attached to C-3' of the pyrrole ring is hydrogen-bonded to the side chain of Asn⁵⁶⁸, the last residue in the hinge region. Asn⁵⁶⁸ is likely to be involved in ATP binding, because the corresponding residue in the insulin receptor tyrosine kinase (Asp¹⁰⁸³) makes a hydrogen bond with one of the ribose hydroxyl groups (26).

In the structures of FGFR1K alone or in complex with ATP (22) or SU4984, the nucleotide-binding loop (the segment between β 1 and β 2 involved in ATP coordination) is poorly ordered. In contrast, the loop is relatively well ordered in the FGFR1K-SU5402 structure, adopting a conformation in which a highly conserved phenylalanine in the loop, Phe⁴⁸⁹, extends

Fig. 6. Interaction of SU5402 with the FGFR1K hinge region. **(A)** Alignment of the amino acid sequences in the hinge region of FGFR1 (residues 563 to 568) and several other receptor tyrosine kinases. Single-letter abbreviations for the amino acid residues are as follows: A, Ala; C, Cys; D, Asp; F, Phe; G, Gly; H, His; K, Lys; L, Leu; M, Met; N, Asn; P, Pro; R, Arg; S, Ser; and Y, Tyr. **(B)** Oxygen-aromatic interactions of the phenyl ring of Phe⁴⁸⁹. The view is approximately 90° from that in Fig. 5, from the right. The coloring is the same as in Fig. 5, with hydrogen atoms (modeled) colored black.

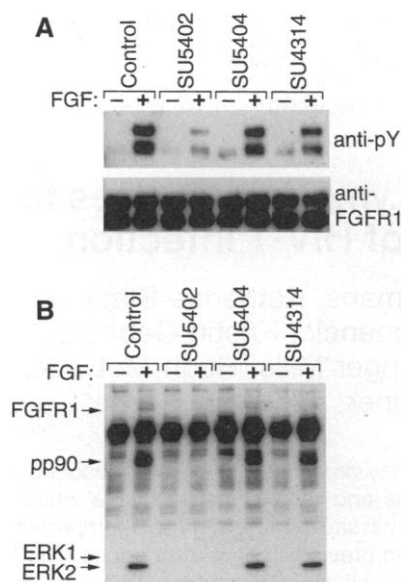
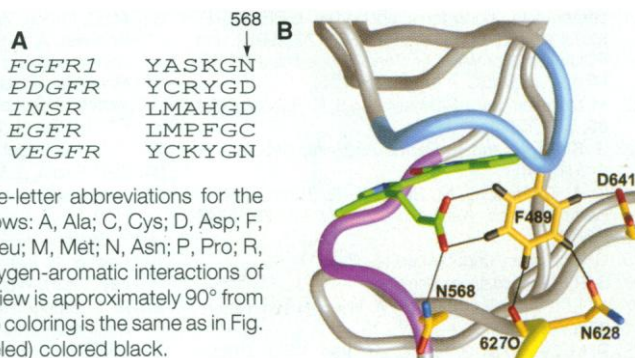


Fig. 7. Importance of carboxyethyl group of SU5402 in inhibition of FGFR1. **(A)** NIH 3T3 cells were treated with 20 μ M of SU5402, SU4314, or SU5404 for 5 min at 37°C and then stimulated with aFGF (100 ng/ml) and heparin (10 μ g/ml) (+) or left unstimulated (-). Cell lysates were immunoprecipitated with antibodies to FGFR1 and analyzed by SDS-PAGE, and then immunoblotted with antibodies to phosphotyrosine (anti-pY) or FGFR1 (anti-FGFR1). **(B)** Portions of the lysates from (A) were analyzed by SDS-PAGE and immunoblotting with anti-pY. The positions of FGFR1, pp90, ERK1, and ERK2 are indicated by arrows.

toward the oxindole, capping the hydrophobic pocket in which the oxindole binds (Figs. 3B and 5B). The difference in position of Phe⁴⁸⁹ in the two FGFR1K-inhibitor structures is \sim 10 Å. The phenyl ring of Phe⁴⁸⁹ in the FGFR1K-SU5402 structure is stabilized by an extensive network of oxygen-aromatic interactions near the plane of the ring (Fig. 6B). Each of the five hydrogen atoms of the phenyl ring is in proximity to an oxygen atom (2.3 to 2.9 Å): the two carboxyethyl oxygens of SU5402, the carbonyl oxygen of Arg⁶²⁷, the side chain oxygen of Asn⁶²⁸, and a side chain oxygen of Asp⁶⁴¹. Asn⁶²⁸ is a highly con-

served residue in the catalytic loop (residues 621 to 628), and Asp⁶⁴¹ is part of a conserved Asp-Phe-Gly sequence motif found in the activation loop (residues 640 to 662) of protein kinases.

The interactions between SU4984 and FGFR1K observed in the crystal structure would not appear to confer specificity: hydrogen bonds are made to backbone groups, and many of the hydrophobic interactions are with conserved residues in the PTK family (Fig. 5A). Consistent with the structural results, SU4984 exhibited rather broad specificity (Fig. 2). The lack of inhibition of the EGF receptor by SU4984 is therefore surprising. The mechanisms of autoinhibition (22, 27) or activation, or both, for the EGF receptor may be sufficiently different to account for the insensitivity to SU4984. Different classes of molecules are potent inhibitors of the EGF receptor (2, 28).

In contrast, SU5402 showed specificity for FGFR1. The hydrogen bond between the side chain amide of Asn⁵⁶⁸ in the hinge region and the carboxyethyl group of SU5402, and the conformational change in the nucleotide-binding loop stabilized by it (Figs. 5B and 6B), evidently confer this specificity. In both the insulin and PDGF receptors, the residue at the position corresponding to Asn⁵⁶⁸ is an aspartic acid (Fig. 6A), which at neutral pH will not form a hydrogen bond with the carboxyethyl group. The vascular endothelial growth factor (VEGF) receptor (FLK) also has an asparagine at this position (Fig. 6A); SU5402 is a potent inhibitor of VEGF receptor in living cells (25). The role of the carboxyethyl-Asn⁵⁶⁸ hydrogen bond in FGFR1 kinase inhibition was evaluated with two compounds similar to SU5402 but which lack the carboxyethyl group. 3-[(3-methylpyrrol-2-yl)methylene]-2-indolinone (SU5404) and 3-[(pyrrol-2-yl)methylene]-2-indolinone (SU4314) were much weaker inhibitors of aFGF-induced tyrosine phosphorylation than SU5402 (Fig. 7).

The amino acid sequence in the kinase hinge region shows considerable variability

among PTKs (Fig. 6A), providing a possible means to achieve specificity in a PTK inhibitor. The FGFR1K hinge region comprises six residues, but the backbone conformation is such that the side chains of Ser⁵⁶⁵ and Lys⁵⁶⁶ point away from the ATP-binding cleft. Furthermore, Gly⁵⁶⁷ is highly conserved, leaving Tyr⁵⁶³, Ala⁵⁶⁴, and Asn⁵⁶⁸ as hinge residues available for interaction with selective PTK inhibitors. Tyr⁵⁶³ is on the periphery of the binding site for SU4984 and SU5402, and would not appear to greatly influence the binding of compounds of this class. In the PDGF receptor, a cysteine is found at the position of Ala⁵⁶⁴. Modeling of cysteine for Ala⁵⁶⁴ in the FGFR1K-SU4984 structure suggests that the cysteine could interact favorably with the phenyl ring of SU4984, which may explain why SU4984 is a more potent inhibitor of the PDGF receptor than of FGFR1.

Crystal structures of the serine/threonine kinases cyclin-dependent kinase 2 (29), casein kinase 1 (30), and cyclic AMP (adenosine 3',5'-monophosphate)-dependent kinase (31) in complex with various inhibitors have been described. These and the present structures show that the ATP-binding pocket, although relatively well conserved in the protein kinase family, will accommodate molecules of different chemical structure which can selectively inhibit protein kinases.

We propose that specific, ATP-competitive PTK inhibitors can be rationally designed upon an oxindole core. The data presented suggest that the oxindole confers high affinity for the adenine binding site in PTKs. Chemical modification of the oxindole at positions 5 and 6 could enhance binding affinity and improve selectivity. Selectivity for individual PTKs could be achieved through interactions between the substituents attached to position 3 of the oxindole and residues of the kinase hinge region. The discovery of a new class of PTK inhibitors and the elucidation of their mechanism of action is significant, because PTK inhibitors are currently used in clinical trials in patients with recurrent malignant glioma as well as other cancers (32).

REFERENCES AND NOTES

1. J. M. Bishop, *Science* **235**, 305 (1987); A. Ullrich and J. Schlessinger, *Cell* **61**, 203 (1990); S. A. Aaronson, *Science* **254**, 1146 (1991).
2. A. Levitzki and A. Gazit, *Science* **267**, 1782 (1995).
3. C. Basilico and D. Moscatelli, *Adv. Cancer Res.* **59**, 115 (1992).
4. M. Jaye, J. Schlessinger, C. Dionne, *Biochim. Biophys. Acta* **1135**, 185 (1992).
5. W. Reardon et al., *Nature Genet.* **8**, 98 (1994); K. M. Neilson and R. E. Friesel, *J. Biol. Chem.* **270**, 26037 (1995).
6. R. Shiang et al., *Cell* **78**, 335 (1994); F. Rousseau et

- al., *Nature* **371**, 252 (1994); M. K. Webster and D. J. Donoghue, *EMBO J.* **15**, 520 (1996).
7. M. C. Naski et al., *Nature Genet.* **13**, 233 (1996).
 8. P. L. Tavormina et al., *ibid.* **9**, 321 (1995); M. K. Webster et al., *Mol. Cell. Biol.* **16**, 4081 (1996).
 9. M. Klagsbrun and E. R. Edelman, *Arteriosclerosis* **9**, 269 (1989); H. Brem and M. Klagsbrun, in *Oncogenes and Tumor Suppressor Genes in Human Malignancies*, C. C. Benz and E. T. Liu, Eds. (Kluwer Academic, Boston, 1993), p. 211; M. Klagsbrun and P. A. D'Amore, *Ann. Rev. Physiol.* **53**, 217 (1991).
 10. J. Adnane et al., *Oncogene* **6**, 659 (1991); F. Penault-Llorca et al., *Int. J. Cancer* **61**, 170 (1995); J. Jacquemier et al., *ibid.* **59**, 373 (1994); S. W. McLeskey, I. Y. Ding, M. E. Lippman, F. G. Kern, *Cancer Res.* **54**, 523 (1994); Y. A. Luqmani et al., *Int. J. Cancer* **64**, 274 (1995); S. Jaakkola et al., *ibid.* **54**, 374 (1993).
 11. H. Y. Leung, W. J. Gullick, N. R. Lemoine, *Int. J. Cancer* **59**, 667 (1994).
 12. F. Yamaguchi, H. Saya, J. M. Bruner, R. S. Morrison, *Proc. Natl. Acad. Sci. U.S.A.* **91**, 484 (1994); R. S. Morrison et al., *J. Neurooncol.* **18**, 207 (1994).
 13. Y. Myoken et al., *Int. J. Cancer* **65**, 650 (1996).
 14. J. J. Li et al., *Cancer* **72**, 2253 (1993).
 15. C. Theillet et al., *Genes Chromosomes Cancer* **7**, 219 (1993).
 16. M. T. Story, *World J. Urol.* **13**, 297 (1995); J. L. Ware, *Cancer Metastasis Rev.* **12**, 287 (1993).
 17. Preparation of 3-[4-(1-formylpiperazin-4-yl)benzylidene]-2-indolinone (SU4984) was as follows: A reaction mixture of 133.15 mg (1.0 mmol) of oxindole, 228.3 mg (1.2 mmol) of 4-(1-formylpiperazin-4-yl)benzaldehyde, and three drops of piperidine in 2 ml of ethanol was stirred at 90°C for 5 hours. After cooling, the precipitate was filtered, washed with cold ethanol, and dried to yield 199.5 mg (65%) of SU4984 as a yellow solid. Nuclear magnetic resonance (NMR) spectroscopy showed that SU4984 exists predominantly in the *trans* configuration (C-2, C-1'), although in the crystal structure, SU4984 is observed in the *cis* configuration. Preparation of 3-[(3-(2-carboxyethyl)-4-methylpyrrol-2-yl)methylene]-2-indolinone (SU5402) was as follows: A reaction mixture of 134.0 mg (1.0 mmol) of oxindole, 217.43 mg (1.2 mmol) of 3-(2-carboxyethyl)-4-methylpyrrol-2-carboxaldehyde, and three drops of piperidine in 3 ml of ethanol was stirred at 90°C for 3 hours. After cooling, the precipitate was filtered, washed with cold ethanol, and dried to yield 172.4 mg (58%) of SU5402 as a yellow solid. NMR spectroscopy showed that SU5402 exists predominantly in the *cis* configuration.
 18. The compounds were dissolved in dimethylsulfoxide (DMSO) as 100 mM stock solutions and stored at 4°C. The compounds were then diluted in DMSO to a concentration 20× the final concentration used in the *in vitro* kinase reactions. FGFR1K (9 μl) [2.2 mg/ml in 10 mM Tris (pH 8) and 10 mM NaCl] was mixed with 1 μl of various concentrations of 20× SU4984 or 20× SU5402, or with 1 μl of DMSO (control). The reaction was started by adding 6 μl of the enzyme-compound mixture to 6 μl of 2× kinase buffer [2 mM ATP/[γ-³²P]ATP (10 μCi/μl), 4 mM MgCl₂ in 10 mM Tris (pH 8), and 10 mM NaCl] at room temperature. At various time points, 2 μl of the reaction mixture was removed and added to 4 μl of 20 mM EDTA to stop the reaction. The reaction products were analyzed by SDS-PAGE (12% gel) and autoradiography. The radioactive bands were excised from the gel, and ³²P incorporation was quantitated by Cerenkov counting with a β counter.
 19. NIH 3T3 cells expressing endogenous FGF receptors were used. Cell culture, cell lysis, immunoprecipitation, and immunoblotting were carried out according to standard procedures. Anti-FGFR1 was described previously [M. Mohammadi et al., *Mol. Cell. Biol.* **16**, 977 (1996)].
 20. [³H]Thymidine incorporation was done as described by Mohammadi et al. (19).
 21. NIH 3T3 cells expressing endogenous PDGF receptors were used. Also used were HER14 cells (33) and NIH1R cells [S. J. Isakoff et al., *J. Biol. Chem.* **271**, 3959 (1996)]. The EGF receptor was immunoprecipitated with monoclonal antibody 108 (33), insulin receptor with monoclonal antibodies (BBE) [N. P. Moller et al., *J. Biol. Chem.* **270**, 23126 (1995)], and PDGF receptor with polyclonal antibodies (PR4) [S. Mori et al., *EMBO J.* **12**, 2257 (1993)].
 22. M. Mohammadi, J. Schlessinger, S. R. Hubbard, *Cell* **86**, 577 (1996).
 23. S. S. Taylor and E. Radzio-Andzelm, *Structure* **2**, 345 (1994).
 24. K. A. Thomas, G. M. Smith, T. B. Thomas, R. J. Feldman, *Proc. Natl. Acad. Sci. U.S.A.* **79**, 4843 (1982).
 25. G. McMahon, unpublished results.
 26. S. R. Hubbard, in preparation.
 27. _____, L. Wei, L. Ellis, W. A. Hendrickson, *Nature* **372**, 746 (1994).
 28. R. M. Lyall et al., *J. Biol. Chem.* **264**, 14503 (1989); B. Margolis et al., *Cell* **57**, 1101 (1989).
 29. W. F. De Azevedo et al., *Proc. Natl. Acad. Sci. U.S.A.* **93**, 2735 (1996); U. Schulze-Gahmen et al., *Proteins Struct. Funct. Genet.* **22**, 378 (1995).
 30. R.-M. Xu, G. Carmel, J. Kuret, X. Cheng, *Proc. Natl. Acad. Sci. U.S.A.* **93**, 6308 (1996).
 31. R. A. Engh, A. Girod, V. Kinzel, R. Huber, D. Bossemeyer, *J. Biol. Chem.* **271**, 26157 (1996).
 32. M. G. Malkin, W. P. Mason, F. S. Lieberman, L. K. Shawver, A. L. Hannah, in *Proceedings of the 32nd Annual Meeting of the American Society of Clinical Oncology*, Philadelphia, PA, 18 to 21 May 1996 (American Society of Clinical Oncology, Philadelphia, PA, 1996), vol. 15, p. 1573.
 33. A. M. Honegger et al., *Cell* **51**, 199 (1987).
 34. S. V. Evans, *J. Mol. Graphics* **11**, 134 (1993).
 35. A. Nicholls, K. A. Sharp, B. Honig, *Proteins* **11**, 281 (1991).
 36. Z. Otwinowski, in *Data Collection and Processing*, L. Sawyer, N. Isaacs, S. Bailey, Eds. (SERC Daresbury Laboratory, Warrington, UK, 1993), p. 56.
 37. A. T. Brünger, *X-PLOR Version 3.1: A System for X-ray and NMR* (Yale Univ. Press, New Haven, CT, 1992).
 38. T. A. Jones, *Methods Enzymol.* **115**, 157 (1985).
 39. Equipment in the structural biology program at the Skirball Institute is partially supported by a grant from the Kresge Foundation. Coordinates have been deposited in the Brookhaven Protein Data Bank, entries 1FGI and 1AGW.

31 January 1997; accepted 11 March 1997

Kinetics of Response in Lymphoid Tissues to Antiretroviral Therapy of HIV-1 Infection

Winston Cavert, Daan W. Notermans, Katherine Staskus, Stephen W. Wietgreffe, Mary Zupancic, Kristin Gebhard, Keith Henry, Zhi-Qiang Zhang, Roger Mills, Hugh McDade, Jaap Goudsmit, Sven A. Danner, Ashley T. Haase*

In lymphoid tissue, where human immunodeficiency virus–type 1 (HIV-1) is produced and stored, three-drug treatment with viral protease and reverse transcriptase inhibitors markedly reduced viral burden. This was shown by *in situ* hybridization and computerized quantitative analysis of serial tonsil biopsies from previously untreated adults. The frequency of productive mononuclear cells (MNCs) initially diminished with a half-life of about 1 day. Surprisingly, the amount of HIV-1 RNA in virus trapped on follicular dendritic cells (FDCs) decreased almost as quickly. After 24 weeks, MNCs with very few copies of HIV-1 RNA per cell were still detectable, as was proviral DNA; however, the amount of FDC-associated virus decreased by ≥3.4 log units. Thus, 6 months of potent therapy controlled active replication and cleared >99.9 percent of virus from the secondary lymphoid tissue reservoir.

In HIV-1 infection, the measurement of viral load in plasma is a useful guide to prognosis and to the efficacy of antiretroviral therapy (1). Ultimately, however, the impact of treatment can only be assessed

completely in the lymphoid tissue (LT) reservoirs, where most of the virus is produced by CD4⁺ T lymphocytes, macrophages, and other lymphoid MNCs and is stored in immune complexes on the surfaces of FDCs. In the asymptomatic stage of infection, the pool of virus on FDCs is at least an order of magnitude greater than that in MNCs (2). In turn, both LT viral compartments exceed by orders of magnitude the quantity of free and cell-associated virus circulating in the bloodstream. In reports published to date, the LT viral pools are little affected by monotherapy with nucleoside analog drugs that inhibit reverse transcriptase (RTIs) (2, 3) and are only moderately reduced by therapy with two or three RTIs (4, 5).

We investigated the effect of treatment with a more potent antiretroviral drug combination on viral burden in serial tonsil

W. Cavert, K. Staskus, S. W. Wietgreffe, M. Zupancic, K. Gebhard, Z.-Q. Zhang, A. T. Haase, Department of Microbiology, University of Minnesota Medical School, Minneapolis, MN 55455, USA.

D. W. Notermans, J. Goudsmit, S. A. Danner, Division of Infectious Diseases, Tropical Medicine, and AIDS and National AIDS Therapy Center, Academic Medical Center, University of Amsterdam, Post Office Box 22700, 1100 DE Amsterdam, Netherlands.

K. Henry, HIV Program, St. Paul–Ramsey Medical Center, St. Paul, MN 55101, USA, and Department of Medicine, University of Minnesota Medical School, Minneapolis, MN 55455, USA.

R. Mills, Abbott Laboratories, Abbott Park, IL 60064, USA.

H. McDade, Glaxo Wellcome Research and Development, Greenford-Middlesex UB6 0HE, UK.

*To whom correspondence should be addressed.